

# Study of enhancement of total cross sections of reactions with ${}^6\text{He}$ , ${}^{6,9}\text{Li}$ nuclei

Yu.E. Penionzhkevich <sup>\*1,2</sup>, Yu.G. Sobolev <sup>1</sup>,  
V.V. Samarin <sup>1,3</sup>, M.A. Naumenko <sup>1</sup>

<sup>1</sup> Joint Institute for Nuclear Research, Dubna, Russia

<sup>2</sup> National Research Nuclear University "MEPhI", Moscow, Russia

<sup>3</sup> Dubna State University, Dubna, Russia

\* e-mail: pyuer@jinr.ru

Received 25.10.2017

The energy dependence of total cross sections of reactions  ${}^6\text{He} + \text{Si}$  and  ${}^{6,9}\text{Li} + \text{Si}$  in the beam energy range 5-30 MeV/nucleon has been measured. An agreement with the published experimental data for the reaction  ${}^6\text{He} + \text{Si}$  was obtained. For the reaction  ${}^9\text{Li} + \text{Si}$  new data in the vicinity a local enhancement of the total cross section was obtained. Theoretical analysis of possible reasons of appearance of this peculiarity in the collisions of nuclei  ${}^6\text{He}$  and  ${}^9\text{Li}$  with Si nuclei has been carried out including the influence of external neutrons of weakly bound projectile nuclei.

**Keywords:** nuclear reactions; neutron rearrangement; time-dependent Schrödinger equation.

## Introduction

It is well known that neutron rearrangement may play an important role in nuclear reactions. The aim of this work is the investigation of the reactions with light nuclei having different external neutron shells. The experiments on measurements of total cross sections were performed for reactions  ${}^6\text{He} + \text{Si}$  and  ${}^9\text{Li} + \text{Si}$ . The interesting results are the unusual wide enhancement of total cross section for  ${}^9\text{Li} + \text{Si}$  reaction as compared with  ${}^{6,7}\text{Li} + \text{Si}$  reactions. The similar weaker behavior was found for  ${}^6\text{He} + \text{Si}$  reaction as compared with  ${}^4\text{He} + \text{Si}$  reaction. The time-dependent quantum approach combined with the optical model was proposed for explanation of these effects.

## Experiment

The experimental setup for the implementation of the transmission method using a multilayer telescope [1] is shown in figure 1. The setup consisted of a system of silicon detectors  $\Delta E_i \times E$ , ( $i = 0-4$ ), Si-telescope (figure 1a), which was used for the measurement of the total cross section  $\sigma_R(E)$  for reactions  ${}^4,6\text{He} + \text{Si}$  and  ${}^{6,7,9}\text{Li} + \text{Si}$  in the energy range  $E \sim 5-50$  MeV/nucleon. The system of  $\Delta E_i \times E$  silicon detectors of the Si-telescope was surrounded by the CsI(Tl)  $\gamma$ -spectrometer of complete geometry for registration of  $\gamma$ -rays and neutrons. The

thin detectors  $\Delta E_0$ ,  $\Delta E_1$  were used to identify the beam particles and determine the particle flux  $I_0$  incident on the target. The position-sensitive detector  $\Delta E_2$  was used as a so-called active collimator [2] which determined the particle flux  $I_0$  incident on the central region of the target. The detectors  $E$ ,  $\Delta E_4$  were used to analyze the products of reactions occurring in the material of the target  $\Delta E_3$ .

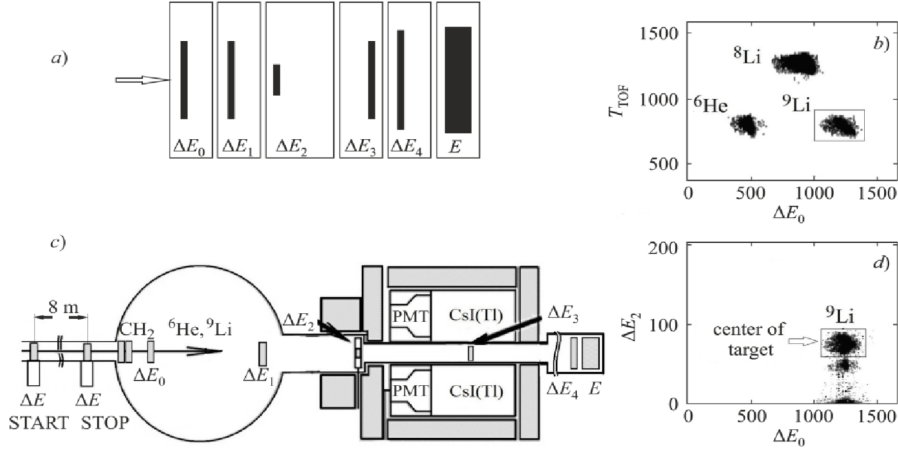


Figure 1. Schematic representation of a multilayer ( $\Delta E_i \times E$ ) Si-telescope (a) and the experimental setup for measuring the reaction cross sections by the method of the  $4\pi$  scintillation  $\gamma$ -spectrometer (c). The spectra ( $\Delta E_0 \times T_{TOF}$ ) are shown used to identify particles  ${}^6\text{He}$  and  ${}^{8,9}\text{Li}$  (b), and ( $\Delta E_0 \times \Delta E_2$ ), used to focus the beam of particles  ${}^9\text{Li}$  on the target (d). Values of energy and time are shown in arbitrary units (channel numbers). Event selection conditions of the flux  $I_0$  of particles  ${}^9\text{Li}$  are shown as contours.

The experiment was performed on the accelerator U400M of the Flerov Laboratory of Nuclear Reactions, JINR. To obtain the secondary beam the fragmentation reaction of  ${}^{11}\text{B}$  beam with the energy  $E_{lab} = 32$  MeV/nucleon on the target  ${}^9\text{Be}$  was used. The secondary beam consisting of a mixture of particles  ${}^6\text{He}$  and  ${}^9\text{Li}$  was formed and purified by the magnetic system of the achromatic fragment separator ACCULINNA [3]. The beam energy was varied by a fragment separator magnetic system, the choice of the thickness of the hydrogen-containing plates of  $\text{CH}_2$  absorbers in the range  $E \sim 15\text{-}50$  MeV/nucleon without significant loss of intensity  $Y$  of the beam of particles. Identification was carried out by energy losses of particles in  $\Delta E_0$ ,  $\Delta E_1$  detectors of the telescope and the time of flight  $T_{TOF}$ . The example of a two-dimensional spectrum  $\Delta E_0 \times T_{TOF}$ , by which the identification of  ${}^6\text{He}$  and  ${}^{6,9}\text{Li}$  particles was performed is shown in figure 1b. In order to reduce the energy uncertainty detectors of different thickness (100, 380, or 500 microns) were used in the experiment depending on the beam energy. Detectors of  $\gamma$  spectrometer recorded  $\gamma$  quanta and neutrons in coincidence with the start signal from the detector  $\Delta E_1$ . The number of events of the reaction  $\Delta R = (I_0 - I)$  of the pre-selected ensemble  $I_0$  of events was determined from the analysis of energy losses in natural Si-target as well as the analysis of gamma and neutron radiation detected by the spectrometer.

The results of measurements of total cross sections for reactions  ${}^{6,7,9}\text{Li} + \text{Si}$  and  ${}^{4,6}\text{He} + \text{Si}$  are presented in figure 2.

The cross section for the reaction with the  ${}^6\text{He}$  nucleus exceeds the cross section with the  ${}^4\text{He}$  nucleus in the entire energy range, which may be explained by the large size of the  ${}^6\text{He}$  nucleus. The measurements showed that the dependence on energy of the total cross section for the reaction  ${}^9\text{Li} + \text{Si}$  has a broad maximum. Enhancement of the cross section for  ${}^9\text{Li}$  nuclei compared to

${}^7\text{Li}$  is observed in the energy range 10–30 MeV/nucleon.

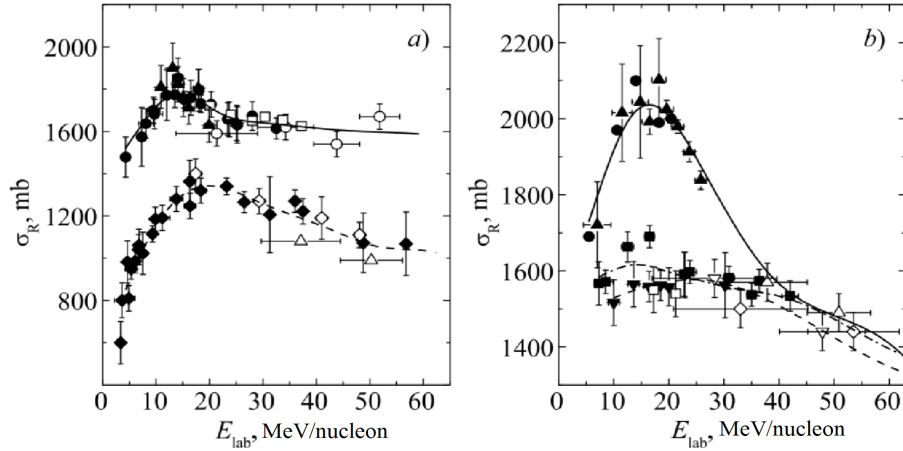


Figure 2. Experimental (symbols) and smoothed (curves) energy dependence of the total cross sections for reactions  ${}^4,6\text{He} + \text{Si}$  (a) and  ${}^6,7,9\text{Li} + \text{Si}$  (b). Filled symbols are the results of measurements using the transmission techniques with multilayer telescope [1, 4], the modified transmission technique of this work and the work [5] (a)  ${}^6\text{He} + \text{Si}$  ( $\blacktriangle$  – this work,  $\bullet$  – [1, 4]),  ${}^4\text{He} + \text{Si}$  ( $\blacklozenge$  – [1, 4]) and (b)  ${}^9\text{Li} + \text{Si}$  ( $\blacktriangle$  this work,  $\bullet$  – [5]),  ${}^7\text{Li} + \text{Si}$  ( $\blacktriangledown$  – [1]),  ${}^6\text{Li} + \text{Si}$  ( $\blacksquare$  – [1]). Open symbols are data for (a)  ${}^6\text{He} + \text{Si}$  ( $\circ$  – [6]),  ${}^4\text{He} + \text{Si}$  ( $\diamond$  – [7],  $\triangle$  – [6]) and (b)  ${}^9\text{Li} + \text{Si}$  ( $\triangle$  – [6]),  ${}^7\text{Li} + \text{Si}$  ( $\nabla$  – [6]),  ${}^6\text{Li} + \text{Si}$  ( $\diamond$  – [6],  $\square$  – [8]). Results of spline [9] smoothing: (a)  ${}^6\text{He} + \text{Si}$  (solid curve),  ${}^4\text{He} + \text{Si}$  (dashed curve); (b)  ${}^9\text{Li} + \text{Si}$  (solid curve),  ${}^7\text{Li} + \text{Si}$  (dashed curve),  ${}^6\text{He} + \text{Si}$  (dash-dotted curve).

## Theory

The analysis of these effects using the microscopic complex folding potential in Ref. [10], as well as within the optical model in Ref. [11] did not provide satisfactory explanation of the observed features in the behavior of the energy dependence of the total cross section. In this study, the potentials of the optical model were modified to take into account the dynamic rearrangement of two external neutrons of projectile nuclei  ${}^6\text{He}$  and  ${}^9\text{Li}$ . The obtained results are in good agreement with the experimental data (figure 3).

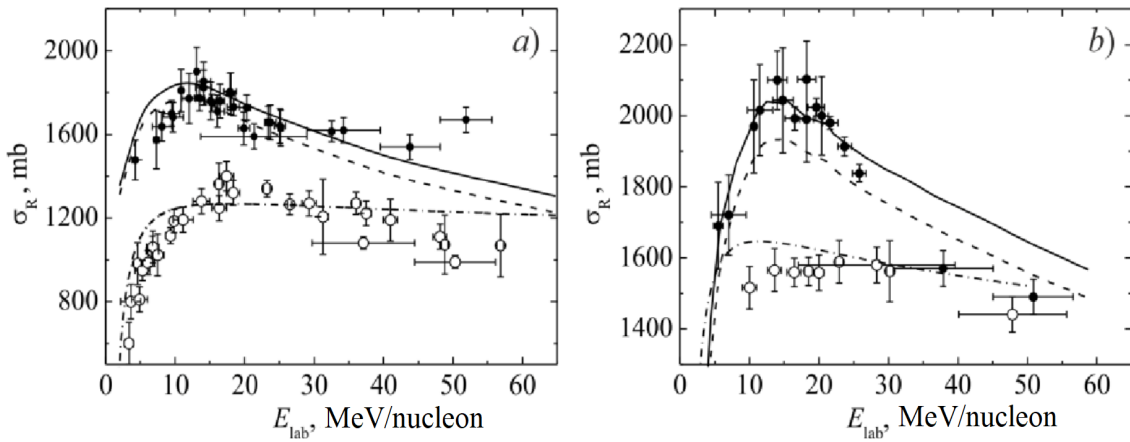


Figure 3. The total cross sections for reactions  ${}^4,6\text{He} + {}^{28}\text{Si}$  (a) and  ${}^7,9\text{Li} + {}^{28}\text{Si}$  (b), symbols are the experimental data:  ${}^6\text{He} + {}^{28}\text{Si}$  and  ${}^9\text{Li} + {}^{28}\text{Si}$  (dots),  ${}^4\text{He} + {}^{28}\text{Si}$  and  ${}^7\text{Li} + {}^{28}\text{Si}$  (circles), curves are the results of calculation within the optical model with the potentials (1), (5): (a) for  $R_a = 5.0$  fm (solid line) and  $R_a = 4.8$  fm (dashed line), (b) for  $R_a = 5.8$  fm (solid line) and  $R_a = 5.6$  fm (dashed line); dash-dotted lines are the results of calculations with the potentials (3), (4) for the reactions  ${}^4\text{He} + {}^{28}\text{Si}$  (a) and  ${}^7\text{Li} + {}^{28}\text{Si}$  (b).

The real part of the potential  $\bar{V}(R)$  for nuclei with "frozen" neutrons was supplemented with the diabatic correction arising from an increase in neutron density between the surfaces of the nuclei as they approach

$$V_d(R, E_{lab}) = \bar{V}(R) + \eta(E_{lab})\delta V_d(R, E_{lab}), \quad (1)$$

where the function  $\delta V_d(R(t), E_{lab})$

$$\delta V_d(R(t), E_{lab}) = \int_{\Omega} d^3r_3 \delta\rho(r_3, t) U_T(|\vec{r}_3 - \vec{r}_2(t)|), \quad (2)$$

$U_T(r)$  is the mean field for neutrons in the target nucleus,  $\delta\rho_1(r_1, t) = \rho_1(r_1, t) - \rho_1^{(0)}(r_1)$ ,  $\rho_1(r_1, t)$  is the probability density of the external neutrons of the projectile nucleus,  $\rho_1^{(0)}(r_1)$  is the same density calculated in the absence of interaction of these neutrons with the target nucleus,  $\Omega$  is the region between the surfaces of the nuclei,

$$\eta(E_{lab}) = \left\{ 1 + \exp \frac{1}{\alpha} \left[ \langle \varepsilon \rangle - \left( \frac{E_{lab}}{A} \right) \right] \right\}^{-1}, \quad (3)$$

$\langle \varepsilon \rangle \sim 10$  MeV is the average kinetic energy of the external neutrons,  $\alpha \sim 2$  MeV. The diabatic correction  $\delta V_d(R, E_{lab})$  reduces the height  $B(E_{lab})$  and shifts to the right the position  $R_B(E_{lab})$  of the Coulomb barrier

$$R_B(E_{lab}) = R_{B,0}(E_{lab}) + \delta R_B(E_{lab}). \quad (4)$$

For the imaginary part of the potential we used the approximation with the exponential dependence

$$W(r) = \begin{cases} -W_1, & r < R_b \\ W_1 \exp\left(-\frac{r-R_b}{b}\right), & r \geq R_b \end{cases}, \quad (5)$$

and the radius  $R_b$ , increasing according to the shift of the barrier position

$$R_b(E_{lab}) = R_a + k\delta R_B(E_{lab}), \quad (6)$$

where  $b = 1$  fm,  $k = 2$ ,  $R_a = 5.8$  fm for the reaction  ${}^9\text{Li} + {}^{28}\text{Si}$ . In the case of reactions with nuclei  ${}^4\text{He}$ ,  ${}^7\text{Li}$  for the real and the imaginary parts of the nuclear potential the Woods-Saxon form was used

$$\text{Re}\{V_N(R)\} \equiv V(R) = -V_0[1 + \exp((R - R_V)/a_V)]^{-1}, \quad (7)$$

$$\text{Im}\{V_N(R)\} \equiv W(R) = -W_0[1 + \exp((R - R_W)/a_W)]^{-1}. \quad (8)$$

For collisions  ${}^{6,7}\text{Li} + {}^{28}\text{Si}$  the parameters  $V_0, R_V, a_V$  of the real part were obtained by fitting the angular distributions of the elastic scattering. The results of calculation of the total cross section of reactions  ${}^{6,7}\text{Li} + {}^{28}\text{Si}$  thus obtained (figure 3) are also in good agreement with the experimental data [1, 6, 8].

The qualitative character of the rearrangement of external neutrons during the approach of nuclei depends on the ratio of the average velocity  $\langle v \rangle$  of the external neutron and the relative velocity  $v_{rel}$  of the nuclei in the process of collision. The average kinetic energy  $\langle \varepsilon \rangle$  of weakly bound neutrons in the nuclei  ${}^6\text{He}$  and  ${}^9\text{Li}$  approximately equals the depth of the potential well of the mean field. Using

estimations  $\langle \varepsilon \rangle \approx 10$  MeV,  $v_1 \approx v_{rel} = \sqrt{2E_{lab}/m_1}$ , where  $E_{lab}$  is the energy of the projectile nucleus with the mass number  $A$  in the laboratory system,  $m_0$  is the atomic mass unit, we obtain the ratio of velocities

$$\frac{v_1}{\langle v \rangle} \approx \gamma = \left[ \frac{E_{lab}}{\langle \varepsilon \rangle A} \right]^{1/2}. \quad (9)$$

At low energies, when  $\langle v \rangle \gg v_1$ ,  $\gamma \ll 1$ , during the flight of the projectile nucleus close to the target nucleus the weakly bound neutrons may, relatively speaking, make a lot of turns around the cores of both nuclei. In the extremely diabatic case (at intermediate energies), when  $\langle v \rangle \ll v_1$ ,  $\gamma \gg 1$ , the neutron may not be able to move to the target nucleus during the time of flight. The value of the parameter  $\gamma$  may be used to estimate the degree of adiabaticity of the collision.

For theoretical description of neutron transfer during collisions of heavy atomic nuclei we used the time-dependent Schrödinger equation (TDSE) approach [12, 13] for the external neutrons combined with the classical equations of motion of atomic nuclei. The evolution of the components  $\Psi_1, \Psi_2$  of the spinor wave function  $\Psi(\vec{r}, t)$  for the neutron with the mass  $m$  during the collision of nuclei is determined by Eq. (10) with the operator of the spin-orbit interaction  $\hat{V}_{LS}(\vec{r}, t)$

$$i\hbar \frac{\partial}{\partial t} \Psi(\vec{r}, t) = \left\{ -\frac{\hbar^2}{2m} \Delta + W(\vec{r}, t) + \hat{V}_{LS}(\vec{r}, t) \right\} \Psi(\vec{r}, t). \quad (10)$$

The centers of nuclei  $\vec{r}_1(t), \vec{r}_2(t)$  with the masses  $m_1, m_2$  move along classical trajectories. We may assume that before contact of the surfaces of spherical nuclei with the radii  $R_1, R_2$  the potential energy of a neutron  $W(\vec{r}, t)$  is equal to the sum of its interaction energies with both nuclei. The initial conditions for the wave functions were obtained on the basis of the shell model calculations with the parameters providing neutron separation energies close to the experimental values.

Examples of the evolution of the probability density of the external neutrons of  ${}^9\text{Li}$  nucleus when colliding with the nucleus  ${}^{28}\text{Si}$  are shown in figure 4.

During a slow (adiabatic) relative motion of the colliding nuclei with  $\gamma = 0.24$  (figure 4a, b, c) the external neutrons (dineutron cluster) of  ${}^9\text{Li}$  nucleus are penetrating the  ${}^{28}\text{Si}$  nucleus and populating the slowly changing two-center ("molecular") states, the probability density for which fills a large part of the volume of the target nucleus. During the rapid (diabatic) relative motion  $\gamma = 1.4$  (figure 4g, h, i) the probability density of neutrons does not have time to fill all the target nucleus and its change is more local (figure 4g, h). After the separation of the nuclei the wave packet in the surface region of the target nucleus remains spreading and rotating with large angular momentum (figure 4i). At intermediate velocities (figure 4d, e, f) there is a transition from the adiabatic regime to the diabatic one.

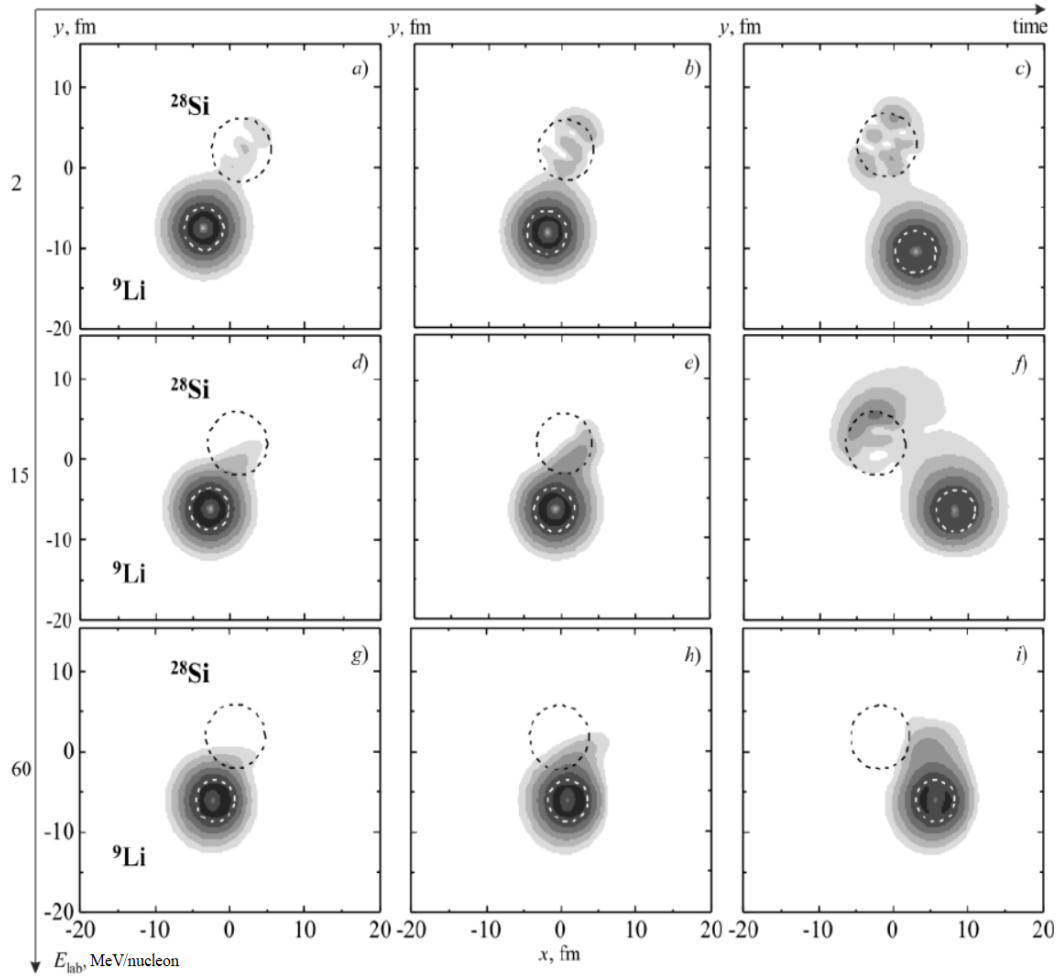


Figure 4. Examples of the evolution of the probability density of external neutrons of  ${}^9\text{Li}$  nucleus during the collision with the nucleus  ${}^{28}\text{Si}$  at energies  $E_{lab} = 2$  MeV/nucleon (a, b, c,  $\gamma = 0.24$ ), 15 MeV/nucleon (d, e, f,  $\gamma = 0.7$ ), and 60 MeV/nucleon (g, h, i,  $\gamma = 1.4$ ). The course of time corresponds to the location from left to right.

## Conclusion

The presented in this paper experimental results of a direct measurement of the total cross section of the reaction ( ${}^6\text{He} + \text{Si}$ ) in the beam energy range 5–40 MeV/nucleon are in good agreement with the known data. For the reaction  ${}^9\text{Li} + \text{Si}$  new data in the vicinity of a local enhancement of the total cross section were obtained. The theoretical analysis of the possible causes of this effect in the collisions of nuclei  ${}^6\text{He}$  and  ${}^9\text{Li}$  with Si nuclei was performed including the influence of external neutrons of weakly bound projectile nuclei. The time-dependent model proposed in the paper shows that the rearrangement of external weakly bound neutrons of nuclei  ${}^6\text{He}$  and  ${}^9\text{Li}$  during the collision changes the real and the imaginary parts of the interaction potential, which may cause a local enhancement in the total cross section of the reaction. This enhancement is most noticeable in the range of energies where the relative velocity of the nuclei is close in magnitude to the average velocity of external neutrons of the studied light weakly bound nuclei.

## Acknowledgments

We express our deep gratitude to the team of researchers of the ACCULINNA experimental facility (FLNR, JINR) as well as to the team of the U400M accelerator (FLNR, JINR) for maintenance of experiments. We also thank A. S. Denikin and A. V. Karpov for fruitful discussions. The work was supported by Russian Science Foundation (RSF), grant No. 17-12-01170.

## References

- [1] Yu.G. Sobolev et al., Bull. Russ. Acad. Sci.: Phys. **69** (2005) 1790.
- [2] Yu.G. Sobolev et al., Instr. Exp. Techn. **54** (2011) 449.
- [3] A.M. Rodin et al., Nucl. Instr. Meth. Phys. Res. B **204** (2003) 114.
- [4] V.Yu. Ugryumov et al., Phys. At. Nucl. **68** (2005) 16.
- [5] Yu.G. Sobolev et al., Phys. Part. Nucl. **48** (2017) 922.
- [6] R.E. Warner et al., Phys. Rev. C **54** (1996) 1700.
- [7] R.E. Warner et al., Phys. Rev. C **74** (2006) 014605.
- [8] A. Ingemarsson et al., Nucl. Phys. A **676** (2000) 3.
- [9] G.I. Marchuk, Methods of Computational Mathematics (Nauka, Moscow, 1980).
- [10] K.V. Lukyanov et al., Bull. Russ. Acad. Sci.: Phys. **72** (2008) 356.
- [11] G.D. Kabdrakhimova et al., Phys. At. Nucl. **80** (2017) 32.
- [12] V.V. Samarin et al., Bull. Russ. Acad. Sci.: Phys. **76** (2012) 450.
- [13] M.A. Naumenko et al., Bull. Russ. Acad. Sci.: Phys. **80** (2016) 264.